JOURNAL OF MATERIALS SCIENCE 26 (1991) 5025–5036

Effect of composition on the transformation behaviour of duplex 316 weld metal

J. J. SMITH*, R. A. FARRAR
Department of Mechanical Engineering, The University of Southampton, Hampshire, UK

Several 316 manual metal arc weld metals produced with commercial and experimental consumables were aged between 600 and 850 °C. This resulted in the dissolution of the δ-ferrite with the appearance of new austenite, $M_{23}C_6$, intermetallics σ, χ and η phase. During transformation, the δ-ferrite becomes progressively enriched in Cr, Mo and Si and, depending on the local composition of the δ-ferrite, eventually transforms to intermetallic σ or χ phases. A transformation model has been developed which indicates that solute diffusion via the δ/γ interface is the controlling mechanism. This enrichment process has been found to be important in controlling the formation of intermetallics. In the weld metals containing controlled residual additions of Ti and Ti + B, ageing resulted in the a fine dispersion of MX phase in the austenitic matrix.

1. Introduction

Austenitic stainless steels have been widely used by petro-chemical and power plant utilities where their good mechanical and high-temperature properties have been exploited. However, numerous studies [1–3] have shown that during high-temperature service, these steels are susceptible to the formation of intermetallic σ phase. The formation of this phase has been shown to result in a loss of creep ductility and toughness [4].

AISI type 316 steel is generally welded with either a consumable of nearly matching composition to the base material 19Cr–12Ni–2Mo, or with a leaner 17Cr–8Ni–2Mo consumable. The composition of the weld metal is controlled to produce a small amount of δ-ferrite, 3%–8% in the deposit; although this is considered beneficial in preventing hot-cracking during fabrication, the δ-ferrite is known to promote the formation of intermetallic σ and/or χ phases.

The factors controlling the transformation of δ-ferrite to intermetallics have been investigated by a number of workers [5–8]. These studies have shown that compositional factors have significant effects on the propensity for the δ-ferrite to transform to intermetallic. However, recent studies by Vitek and David [9] have disputed the importance of compositional factors in controlling the $\delta \rightarrow \sigma$ reaction and they concluded that the transformation is limited by nucleation factors.

In the present investigation, a number of duplex weld metals were aged between 600 and 850 °C. With the exception of one 19Cr–12Ni–2Mo and one 17Cr–8Ni–1Mo consumable, the manual metal arc deposits were produced using basic and rutile-coated consumables of the 17Cr–8Ni–2Mo type. Although the 17Cr–8Ni–2Mo deposits were of the same nominal composition, the deposits contained small but significant changes in C, Cr, Mo and Si and controlled residual elemental levels. The objectives of this research were to study the effect of these small compositional changes on the microstructural, and micro-compositional changes in the δ-ferrite, and its subsequent ageing behaviour.

2. Experimental procedure

2.1. Welding procedure and chemical analysis

All weld metal pads 150 mm high, 200 mm long and 150 mm wide were deposited on heavy base plates by the manual metal arc process. Each block was constructed from approximately 150 weld passes. The welds were deposited using 4 mm electrodes in the downhand position with currents of 85–140 A, d.c. electrode positive.

The chemical analysis of the weld metals and the as-deposited δ-ferrite contents are shown in Table I. The nominal δ-ferrite contents were within 3%–11%. Fig. 1 shows the bulk compositions of the deposits in relation to the Schaeffler diagram. Weld metals BW13 and BW14 were deposited using rutile 17Cr–8Ni–2Mo Metrode RCF electrodes. These electrodes also contained further additions of B and Ti + B, respectively, to assess the effects of controlled residual elements (CRE) on the transformation behaviour. Weld metal BW17 was an experimental rutile 17Cr–8Ni–2Mo Metrode RNF electrode. The electrode was based on a pure iron core wire with the

* *Present address*: Structural Integrity Division, E.R.A Technology, Leatherhead, Surrey, UK.

0022–2461/91 $03.00 + .12

TABLE I Chemical composition (wt %) and δ-ferrite content

Deposit	% δ	C	Si	Mn	Cr	Mo	Ni	Nb	Ti	V	N	B
BW13	4.7	0.080	0.29	2.16	17.4	1.74	8.5	0.070	0.024	0.11	0.053	0.005
BW14	5.9	0.092	0.51	2.31	18.2	1.84	8.7	0.040	0.031	0.11	0.050	0.004
BW17	11.4	0.077	0.44	2.20	18.6	1.80	9.7	0.009	0.020	0.02	0.040	0.003
BW18	9.8	0.079	0.68	1.90	16.4	1.80	8.4	0.017	0.020	0.06	0.024	0.001
BW20	5.3	0.050	0.24	1.17	18.5	2.17	11.4	0.040	0.019	0.06	0.079	0.001
BW24	4.2	0.075	0.41	2.08	17.8	1.10	8.6	0.050	0.040	0.02	0.048	0.002

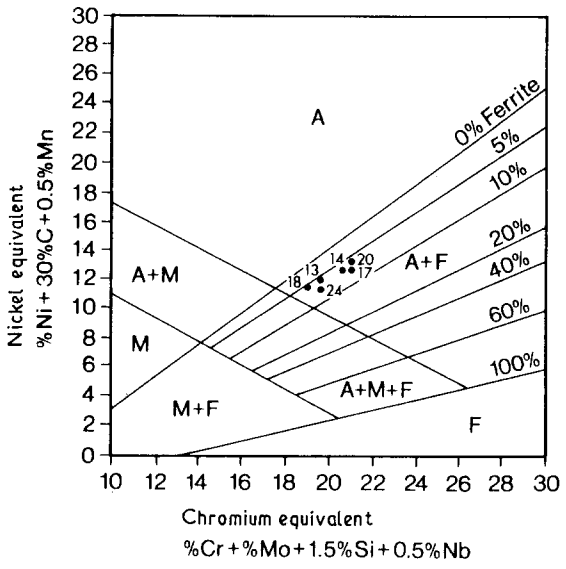

Figure 1 Bulk composition of weld metals in relation to the Schaeffler diagram. A, austenite; F, ferrite; M, martensite.

alloying elements contained in the coating. Weld metal BW18 was deposited using 17Cr–8Ni–2Mo Armex GTR electrodes, a variant of Armex GT a type which has been widely used in the power generating industry. Weld metal BW20 was deposited using rutile 19Cr–12Ni–2Mo Soudinox B 316 electrodes. BW24 was an experimental rutile 17Cr–8Ni–1Mo Metrode electrode.

2.2. δ-Ferrite transformation

The δ-ferrite contents of the as-deposited and aged specimens were determined magnetically using a "Magne-Gage" instrument. This was calibrated with primary and secondary standards according to the AWS A4–2–74 procedure. In order to minimize errors, a template of the specimen was placed on the surface to ensure that the specimens were located in precisely the same position and orientation relative to the magnetic probe before and after heat treatment. Readings were made at eight different locations on the charpy specimens which were numbered so that the precise changes in the δ-ferrite content could be calculated.

2.3. Preparation and examination

Extraction replicas and thin foils were examined in a JEOL 100CX scanning transmission electron microscope with STEM and energy dispersive X-ray (EDX) analysis facilities. For all micro-composition analyses, standard conditions of 50 μm condenser aperture, a nominal electron probe size of 10 nm and a window thickness of 8 μm with a resolution of 160 keV (at Mn K_α) were employed. Typical micro-compositional analyses were determined after accumulating 50 000 counts in 100 s. The foils were tilted so that the phase boundary was parallel to the electron beam to minimize any systematic error. The local composition of the primary δ-ferrite was determined from approximately 100 δ-ferrite measurements. Under these operating conditions, the standard error in the analysis arising from the counting statistics were < 0.30 at % for Ni and 0.40 at % for Cr. The spatial resolution (electron beam width plus beam broadening) has been estimated to be approximately 40 nm for 100 keV electrons in a 150 nm thick foil. Further "K corrections" for the equipment as recommended by Farrar and Thomas [6] were employed.

2.4. X-ray diffraction

Small pieces of weld metal were dissolved electrolytically in 10% HCl–methanol solution. The residues were dried, weighed and mixed with 25% by weight of ZnO, ZnO being an internal standard. The extractions were analysed using a Siemens D500 diffractometer using Cr K_α radiation.

3. Results

3.1. As-welded metallography

For δ-ferrite levels up to approximately 6% (BW13, 14, 20 and 24), the distribution was characterized by columns of skeletal δ-ferrite aligned along the primary dendrite growth axis, parallel to the heat flow axis or columnar growth direction, Fig. 2a. There was extensive interlocking of the secondary arms such that the δ-ferrite appeared as a semi-continuous network. This type of δ-ferrite morphology has been previously identified and characterized by David [10] as vermicular δ-ferrite. Increasing the δ-ferrite levels above 8% (BW17 and 18) produced a gradual transition in morphology from the vermicular to the lacy type [10] characterized by long interlocking columns, Fig. 2b.

In all the weld metals, the columnar grain size was typically 50–125 μm, with the δ-ferrite distribution creating a subgrain size of 10–15 μm.

3.2. Ageing metallography

3.2.1. Microstructural changes in the δ-ferrite

3.2.1.1. Ageing at 600 °C. In all the deposits, the rate of dissolution of the δ-ferrite was slow. After ageing for

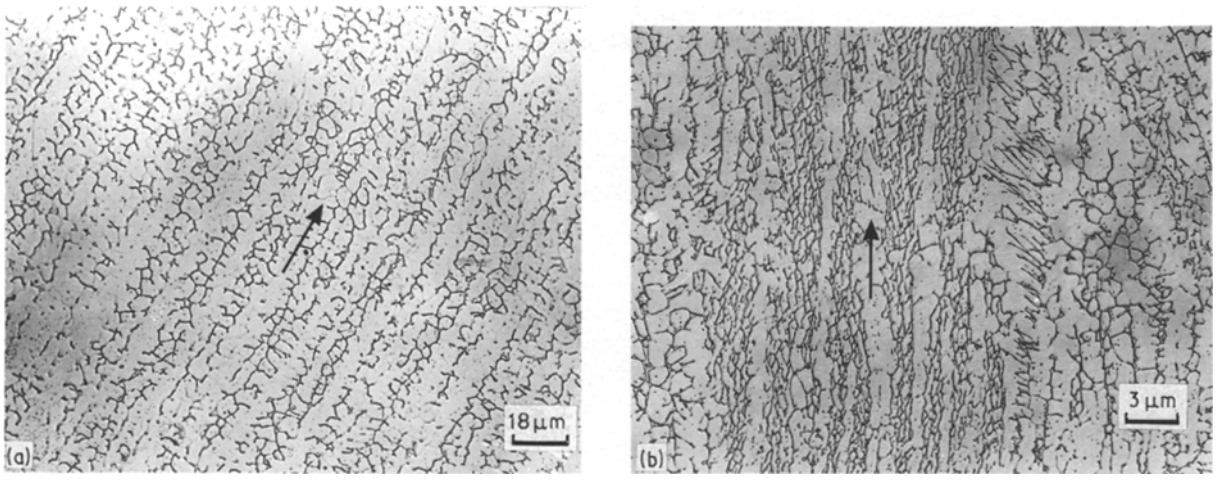

Figure 2 Optical micrographs showing (a) as-welded vermicular δ-ferrite, (b) as-welded lacy δ-ferrite with arrows indicating direction of solidification.

30 h at 600 °C, the δ-ferrite was similar to the as-welded state but with some spheroidization of the dendrite tips, Fig. 3a. Electron microscopy showed that the δ/γ boundaries were outlined by thin semi-continuous films of $M_{23}C_6$ carbide, Fig. 3b. After longer ageing times these morphological changes became more pronounced, producing a gradual breakdown of the interlocking δ-ferrite substructure and causing the carbide morphology to show some tendency to spheroidize and become less continuous. In BW17 after 2500 h, intermetallic σ phase precipitated in the δ-ferrite, Fig. 3c. The intermetallics were coarse and typically 2–3 μm in size, they were also morphologically similar to the original δ-ferrite. This type of intermetallic morphology has been previously characterized by Gill *et al.* [8] as dendritic. The type and relative amount of precipitates formed during ageing at 600 °C of deposits BW13, 14, 17 and 18 are shown in Fig. 4.

3.2.1.2. Ageing at 700 °C. The microstructural transformations at 700 °C were similar to that observed at 600 °C, except for an increase in the rate of dissolution of the δ-ferrite, Fig. 5a. In all the deposits, ageing at 700 °C induced rapid precipitation of $M_{23}C_6$ carbides along the δ/γ boundaries. A number of different $M_{23}C_6$ morphologies were identified including faceted, non-faceted and Widmanstätten plate types. After ageing for 3 h, the δ-ferrite appeared less continuous due to the spheroidization of the secondary dendrite arms. Further ageing resulted in the progressive dissolution of the δ-ferrite, with BW20 and BW13 trans-

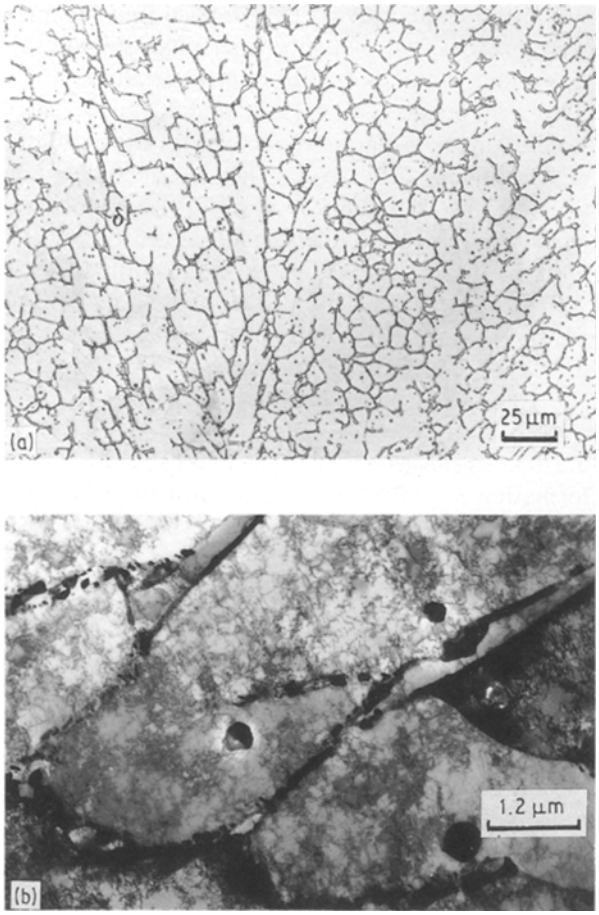

Figure 3 (a) Optical micrograph showing slight spheroidization of secondary arms in BW17 after 30 h at 600 °C, (b) electron micrograph showing semi-continuous films of $M_{23}C_6$ carbide at the δ/γ boundaries after 30 h at 600 °C, (c) optical micrograph showing the δ-ferrite transforming to intermetallic after 2500 h at 600 °C.

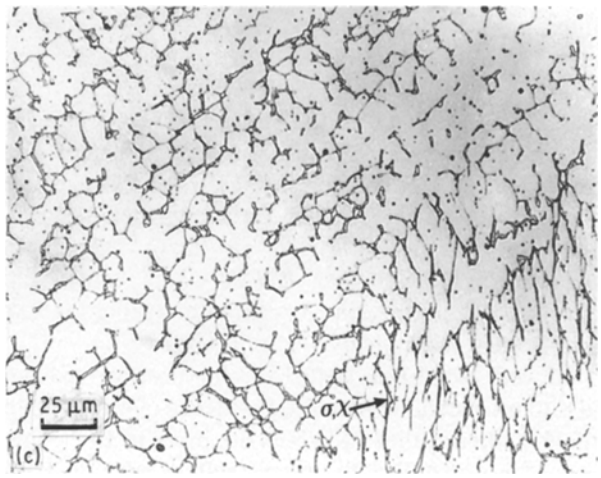

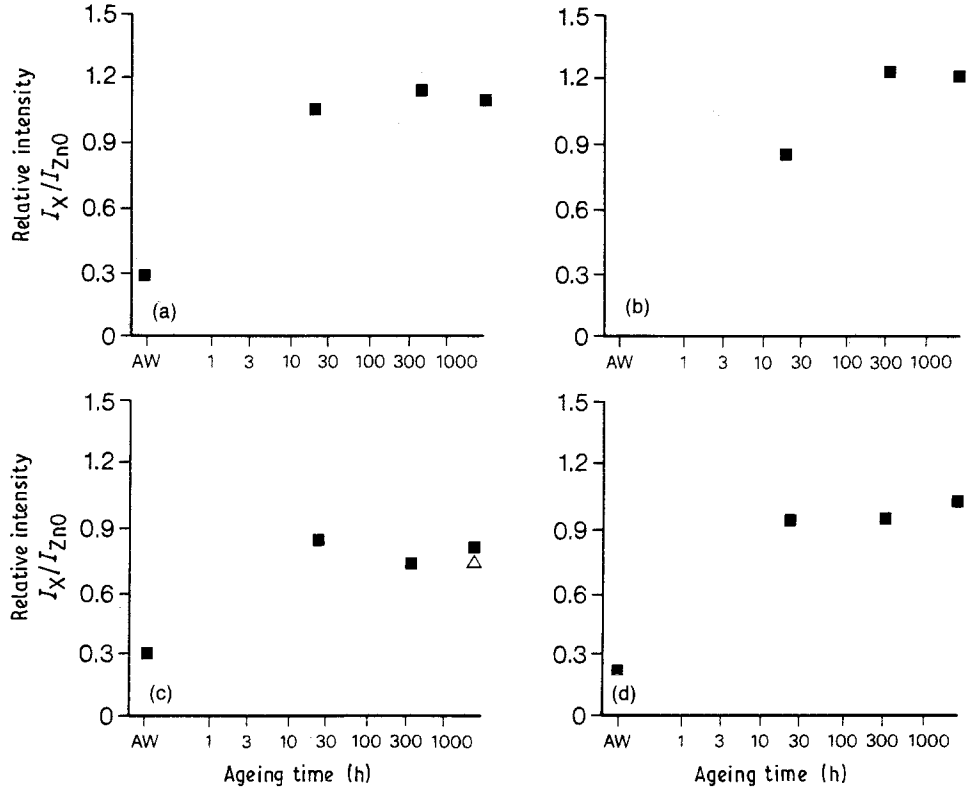

Figure 4 Type and relative amount of precipitation detected by bulk extraction X-ray analysis for deposits (a) BW13, (b) BW14, (c) BW17, (d) BW18, after ageing at 600 °C. (■) $M_{23}C_6$, (△) σ.

forming the fastest and slowest, respectively, Fig. 5a. Detailed transmission electron microscopy showed that the δ/γ transformation occurred by two mechanisms: (i) the migration of the δ/γ interface into the δ-ferrite, Fig. 6a, and (ii) a discontinuous precipitation transformation $\delta \rightarrow \gamma + M_{23}C_6$, Fig. 6b. During the discontinuous transformation, the δ/γ boundary advances with the growing tips of the $M_{23}C_6$ carbides until at some point, the δ/γ boundary advances ahead of the carbides.

Micro-compositional traverses across a number of partially transformed δ-ferrite laths showed that the new austenite γ_n was depleted in Cr and Mo and slightly enriched in Ni compared to the original γ austenitic matrix, Fig. 7.

In all the deposits, after sufficient time at temperature, the remaining δ-ferrite which was enriched in Cr, Mo and Si transformed to new austenite and/or intermetallic σ or χ phases, Fig. 6c. The ageing time required to nucleate intermetallics σ or χ varied considerably with weld metals BW20 and BW13 transforming the fastest and the slowest, respectively. The type and relative amounts of precipitate formed during ageing of weld metals BW13, 14, 17 and 18 are shown in Fig. 5b–e. In BW17, the intermetallics were observed after ageing for 3 h at 700 °C. This was in contrast to BW13 and BW24 where only small amounts of intermetallic formed after ageing for 1000 and 3000 h, respectively.

In weld metal BW20, the δ-ferrite transformed rapidly to intermetallic with little evidence of migration of the δ/γ interface into the δ-ferrite prior to the formation of intermetallic. The intermetallics were observed to nucleate at the original δ/γ boundary and then on further ageing, consume the remaining δ-ferrite. However, in BW13, 14, 17 and 18 the intermetallics tended to nucleate preferentially in regions where significant migration had occurred. This implied that the migration process and possibly interfacial stresses were important in the formation of intermetallics.

In weld metals BW14, 17, 18 and 20, further ageing resulted in the progressive increase in the amount of intermetallics, Fig. 5b–e. The intermetallics were coarse, typically 2–3 μm in size, and were morphologically similar to the intermetallics formed at 600 °C.

In BW13, 14 and 18, after ageing for 1000 h at 700 °C, a lenticular phase precipitated along the prior δ/γ boundaries. These were identified by selected-area diffraction as AB_2 type intermetallic η phases.

3.2.1.3. Ageing at 850 °C. The microstructural transformation at 850 °C were rapid with the widespread dissolution of the δ-ferrite and the appearance of $M_{23}C_6$ carbide and intermetallics σ and χ phase, Fig. 8a–e. Initially on ageing, the secondary dendrite arms transformed faster than the primary dendrite core. During this stage, the tips of the secondary dendrite arms became spheroidized and/or detachment occurred by the formation of a neck at the base of the dendrite arms, Fig. 9a. This resulted in the breakdown of the interlocking branches of the δ-ferrite leaving a primary aligned dendrite core.

In all the deposits, ageing for 1 h at 850 °C resulted in the rapid precipitation of the $M_{23}C_6$ carbide along the δ/γ boundaries. These carbides were non-faceted

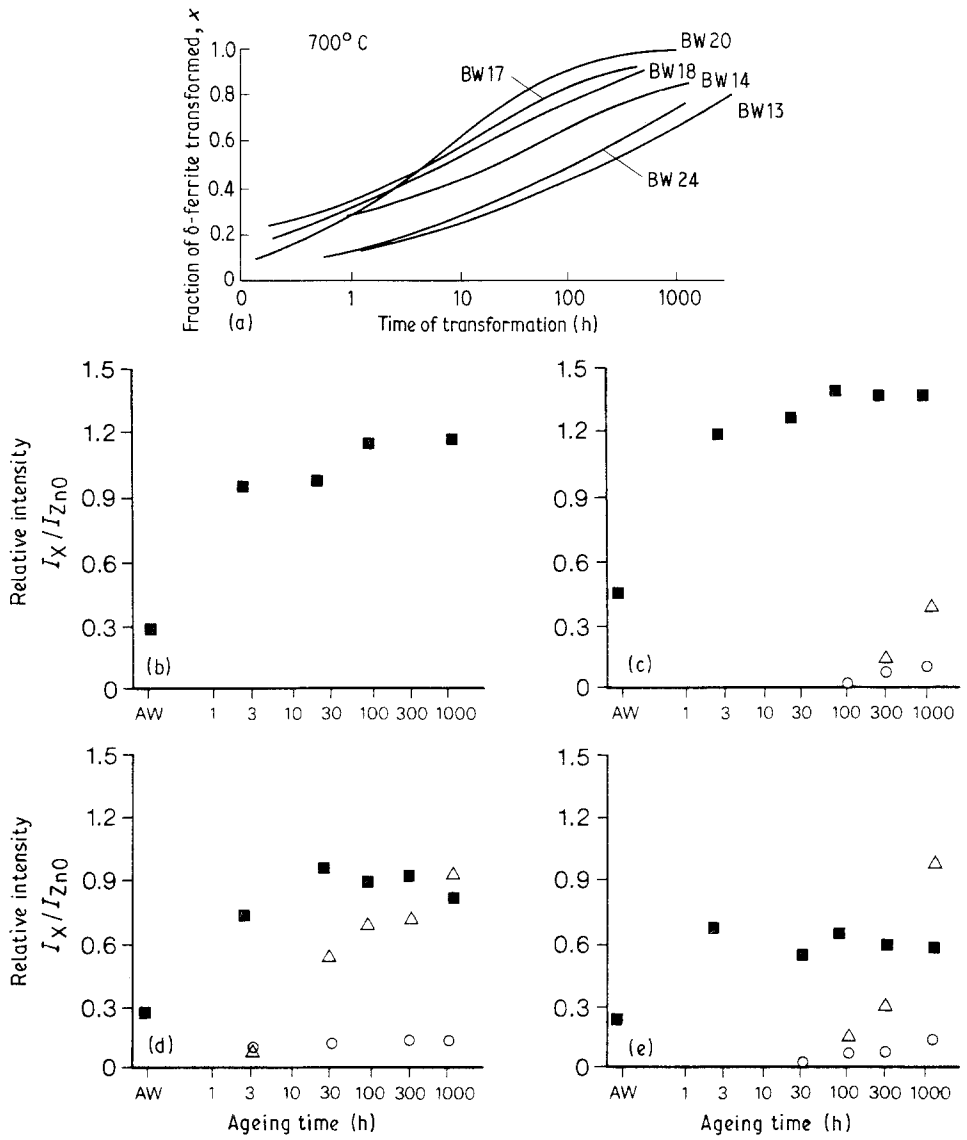

Figure 5 (a) Fraction of δ-ferrite transformed on ageing at 700 °C, (b–d) type and relative amount of precipitation detected by bulk extraction X-ray analysis for deposits (b) BW13, (c) BW14, (d) BW17, (e) BW18, after ageing at 700 °C. (■) $M_{23}C_6$, (△) σ, (○) χ.

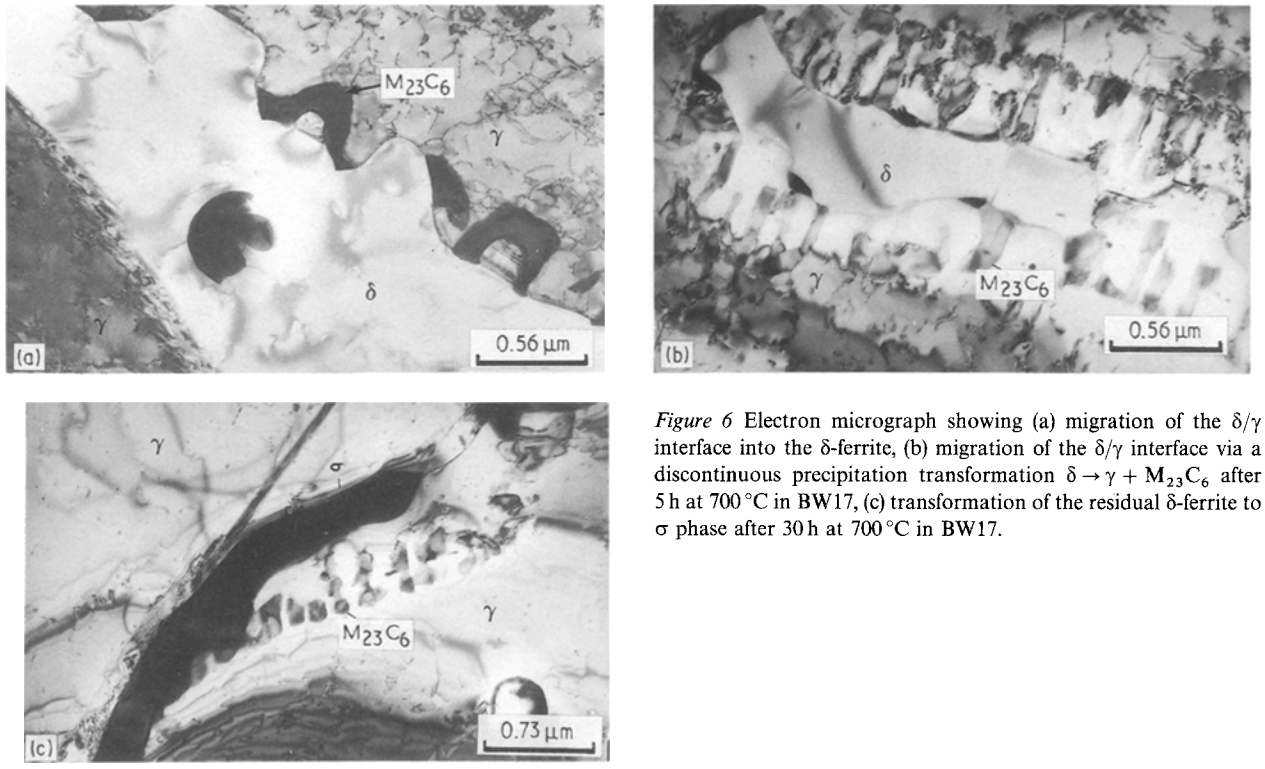

Figure 6 Electron micrograph showing (a) migration of the δ/γ interface into the δ-ferrite, (b) migration of the δ/γ interface via a discontinuous precipitation transformation $\delta \rightarrow \gamma + M_{23}C_6$ after 5 h at 700 °C in BW17, (c) transformation of the residual δ-ferrite to σ phase after 30 h at 700 °C in BW17.

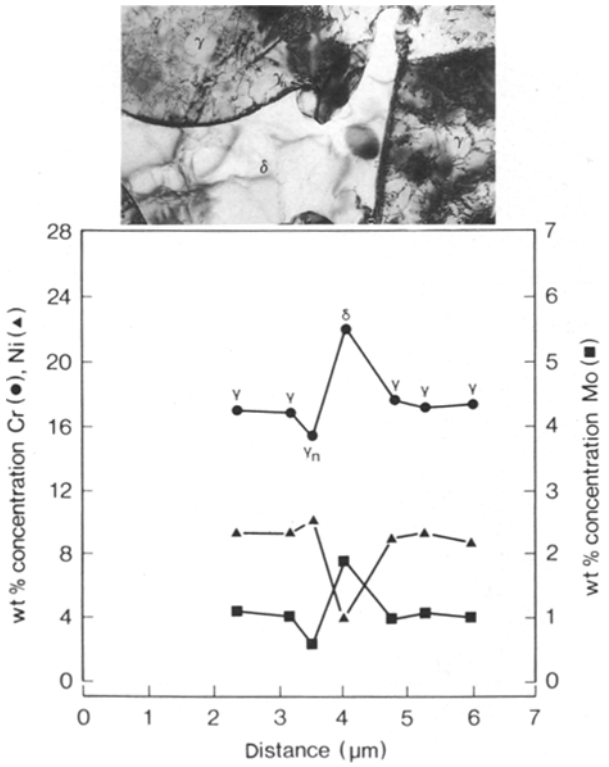

in appearance and tended to be more discrete and discontinuous compared to those formed at 700 °C.

Similar to the ageing studies at 700 °C, ageing at 850 °C resulted in the migration of the δ/γ into the δ-ferrite and/or the discontinuous precipitation reaction $\delta \rightarrow \gamma + M_{23}C_6$. In all the deposits, in regions where the δ/γ boundary had advanced ahead of the $M_{23}C_6$, the carbides were observed to dissolve and spheroidize.

In all the deposits, the precipitation of intermetallics occurred after shorter times compared to ageing at 700 °C. In BW17 and 20, transformation to intermetallics was extremely rapid and occurred after only 1 h at 850 °C. After ageing for 8 h, there was a progressive dissolution of the dendrite cores with the appearance of σ phase in all deposits, Fig. 9b. In BW 17 and 20, the rapid dissolution of the δ-ferrite resulted in the formation of large quantities of intermetallics. The intermetallics were typically 3–5 μm in

Figure 7 Microcompositional traverse across migrating δ/γ boundary after 12 h at 700 °C. γ_n, newly formed austenite.

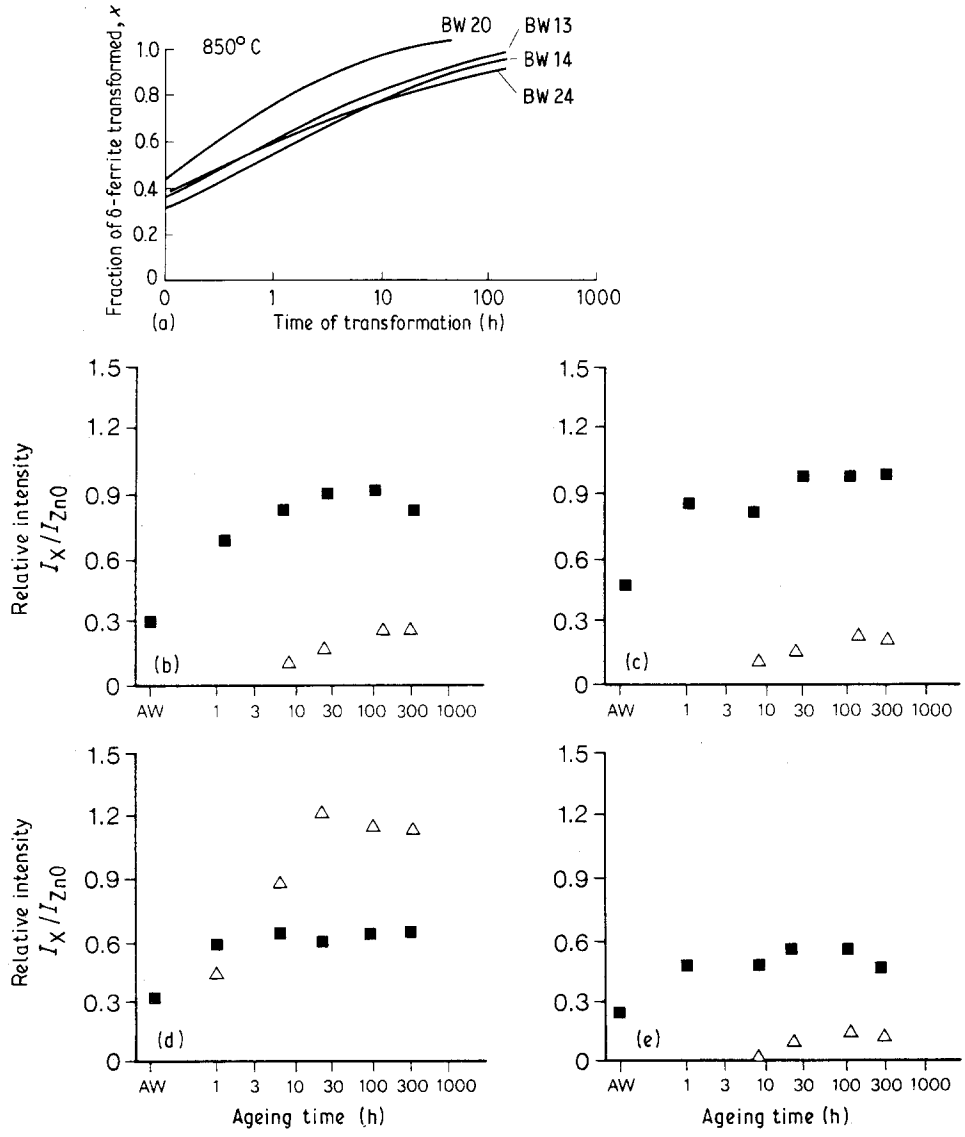

Figure 8 (a) Fraction of δ-ferrite transformed on ageing at 850 °C, (b–d) type and relative amount of precipitation detected by bulk extraction X-ray analysis for deposits (b) BW13, (c) BW14, (d) BW17, (e) BW18, after ageing at 850 °C. (■) $M_{23}C_6$, (△) σ.

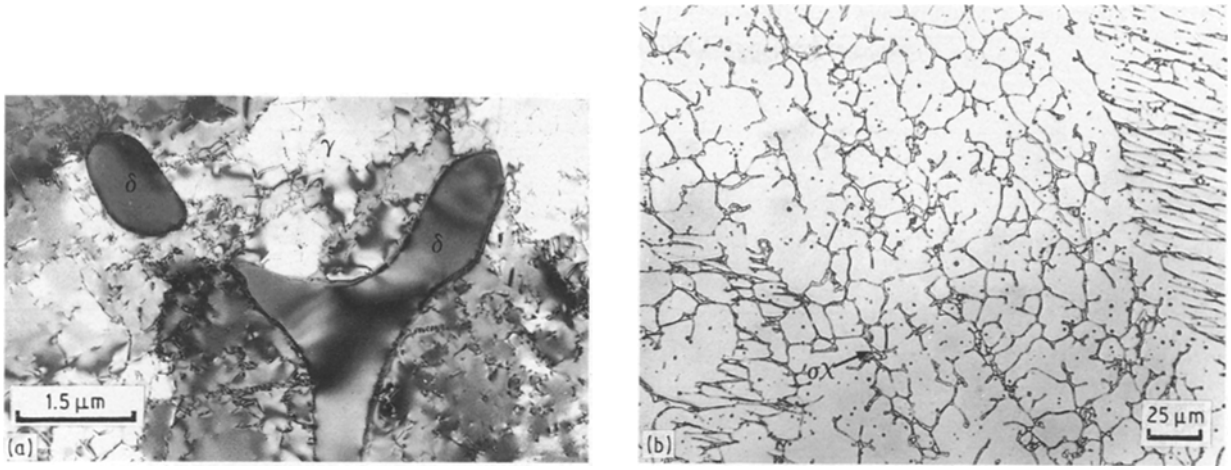

Figure 9 (a) Electron micrograph showing the detachment of the secondary dendrite arms at 850 °C, (b) optical micrograph showing the rapid dissolution of the δ-ferrite with the appearance of σ phase.

size and were spheroidized and discontinuous. In the other weld deposits the amount of intermetallic present was small. The type and relative amount of precipitates formed during ageing of deposits BW13, 14, 17 and 18 are shown in Fig. 8b–e.

Micro-compositional traverses across a number of the sigma particles showed that the new austenite adjacent to the σ/γ interface was significantly depleted in Mo and to a smaller extent in Cr, Fig. 10.

3.2.2. *Microstructural changes in the austenite*

In the weld metals containing the controlled residual element (CRE) additions (BW13 and 14), small particles, approximately 0.02–0.04 μm in size, precipitated on dislocations within the austenite. These were identified by selected-area diffraction as MX type precipitates, Fig. 11.

3.3. Micro-compositional analysis

The micro-composition of the primary δ-ferrite dendrites in the as-welded condition are shown in Table II. The δ-ferrite was enriched in Cr and Mo and depleted in Ni and Mn due to segregation during solidification. In addition to these elements, in BW18 approximately 1.1 wt % Si had segregated to the δ-ferrite (this compared with 0.5 wt % Si in the other weld deposits). After ageing for 0.5 and 70 h at 700 °C, the δ-ferrite was re-analysed in order to assess any shift in composition. In all the weld metals, the δ-ferrite was leaner in Cr and Mo relative to the as-welded values, Table II. After ageing for 70 h at 700 °C, this effect was reversed with the residual δ-ferrite becoming enriched in Cr and Mo. In addition in BW18, the δ-ferrite was further enriched in Si compared to the as-welded condition, and now contained 1.7 wt % Si.

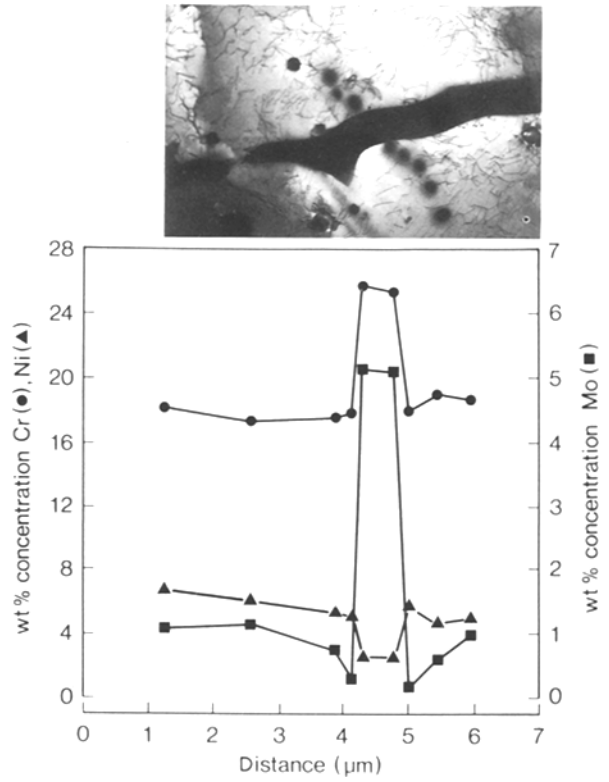

Figure 10 Microcompositional traverse across σ/γ interface.

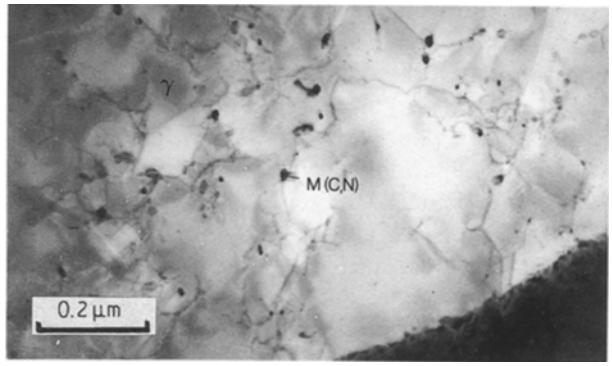

Figure 11 Electron micrograph showing the precipitation of M(CN) carbonitrides on dislocations in the austenite in BW14.

4. Discussion

In this study a number of duplex deposits within the 316 specification have been studied. In all the deposits,

TABLE II Microcomposition of the δ-ferrite in the as-welded and aged conditions

	As-welded		Aged 0.5 h at 700 °C		Aged 70 h at 700 °C	
Deposit	Cr	Mo	Cr	Mo	Cr	Mo
BW13	19.75 ± 0.93	2.25 ± 0.67	17.65 ± 0.75	1.20 ± 0.58	19.84 ± 1.17	1.82 ± 0.43
BW14	21.50 ± 0.87	2.45 ± 0.64	17.93 ± 0.70	0.65 ± 0.41	19.45 ± 0.92	1.21 ± 0.56
BW17	22.35 ± 1.11	2.50 ± 0.83	21.1 ± 0.92	1.75 ± 0.47	22.92 ± 1.64	2.71 ± 0.69
BW18	20.26 ± 0.72	2.29 ± 0.62	18.35 ± 0.87	1.56 ± 0.45	20.58 ± 1.03	1.97 ± 0.62
BW20	21.81 ± 0.99	4.81 ± 0.64	20.57 ± 0.76	4.07 ± 0.48	22.84 ± 1.33	4.90 ± 0.82
BW24	20.14 ± 0.97	1.23 ± 0.59	17.51 ± 0.49	0.61 ± 0.46	18.11 ± 1.09	0.87 ± 0.47

ageing between 600 and 850 °C resulted in the progressive dissolution of the δ-ferrite with the appearance of new austenite, $M_{23}C_6$ and intermetallic σ, χ and η phases. However, the weld metals studies showed considerable differences in the rate of dissolution of the δ-ferrite and sensitivity to intermetallic formation. The following sections therefore discuss the effect of ageing time, temperature and composition on the transformation behaviour.

4.1. $\delta \rightarrow \gamma$ transformation

In all the deposits, ageing resulted in the rapid precipitation of $M_{23}C_6$ at the δ/γ boundaries. The transformation of $\delta \rightarrow \gamma + M_{23}C_6$ involved both discontinuous and continuous modes of precipitation. In BW17, ageing between 700 and 850 °C, resulted in the formation of cells of $M_{23}C_6$ and new austenite via a discontinuous transformation mechanism, Fig. 6b. Growth occurred by the movement of cells with the migrating δ/γ boundary. Beckitt [2] observed a similar transformation behaviour in a duplex steel at 700 °C. During this type of transformation the growth of the cells are known to be controlled by solute diffusion (Cr, Mo and Fe) along the grain boundaries and carbon diffusion from the matrix. At some point during this transformation, the discontinuous precipitation process breaks down resulting in the migration of the δ/γ interface away from the cells. From a detailed analyses of these reactions in a Nimonic 80A alloy, Voice and Faulkner [11] have reported that this transition occurs when the rate of supply of substitutional atoms to the grain boundary exceeds that of carbon diffusion. In BW17 at lower ageing temperatures of 600 °C and in other weld metals studied at all temperatures, the discontinuous mode of precipitation did not occur to any significant extent and the transformation behaviour was dominated by a continuous mode of precipitation. During this mode of precipitation, the δ/γ boundary migrates ahead of the $M_{23}C_6$ carbides. The reason why the discontinuous reaction occurs in one weld metal but not in another of the same nominal composition is uncertain. These differences in behaviour are probably related to the sensitivity of the reaction to carbide composition and morphology and/or the influence of ternary or residual elements on the boundary mobility.

4.2. Micro-compositional changes across the δ/γ boundary

The STEM micro-compositional traverses across the δ/γ interface showed that the new austenite was depleted in Cr and Mo and enriched in Ni compared to the matrix austenite composition. In addition, the micro-compositional measurements in the δ-ferrite showed a gradual enrichment in Cr and Mo with increasing ageing time, Table II.

From these compositional measurements, it is possible to model the dissolution of the δ-ferrite. For a unit area of the δ/γ interface to advance a distance, dx, into the δ-ferrite, solute is transferred from the austenite to the δ-ferrite via the δ/γ interface, Fig. 12.

$$v = \mathrm{d}x/\mathrm{d}t = D/(C_\delta - C_{\delta\gamma})\mathrm{d}c/\mathrm{d}x \quad (1)$$

where $C_{\delta\gamma}$ is the concentration of solute M at the δ/γ interface, C_δ is the concentration of solute M in the δ-ferrite, C_γ is the concentration of solute M in the austenite and D is the diffusivity.

If the concentration profile is simplified

$$\mathrm{d}c/\mathrm{d}x = (C_\gamma - C_{\delta\gamma})/L \quad (2)$$

where L is the characteristic diffusion distance and is approximately $2(Dt)^{1/2}$.

Substitution into Equation 1 and integrating between the limits $(x, 0)$ and $(0, t)$, the migration distance is given by

$$x = (C_\gamma - C_{\delta\gamma})(Dt)^{1/2}/(C_\delta - C_{\delta\gamma}) \quad (3)$$

Assuming that the dissolution of the δ-ferrite is controlled by chromium diffusion, from the measurements obtained on BW20, Fig. 7, $Cr_\gamma = 17.7$ wt %, $Cr_{\delta\gamma} = 15.2$ wt %, $Cr_\delta = 22.5$ wt % $X_{actual} = 0.55$ μm, where $D_{Cr_\gamma} = 5.6 \times 10^{-19}\ m^2\ s^{-1}$ [12] and $D_{Cr_{\delta\gamma}} = 2.49 \times 10^{-17}\ m^2\ s^{-1}$ [13], $X_{theoretical}$ is estimated to be 0.054 and 0.36 μm for Cr diffusion in the austenite and the δ/γ boundary, respectively. From these data it is apparent that there is poor correlation between the experimental and calculated boundary migration distance for diffusion in the austenite. However, the calculated migration distance for diffusion at the δ/γ boundary is of the same order of magnitude as the observed shift in the interface. This indicates that the δ/γ transformation is controlled by diffusion along the δ/γ boundary in preference to that previously suggested of diffusion in the austenite [6, 14]. This may be

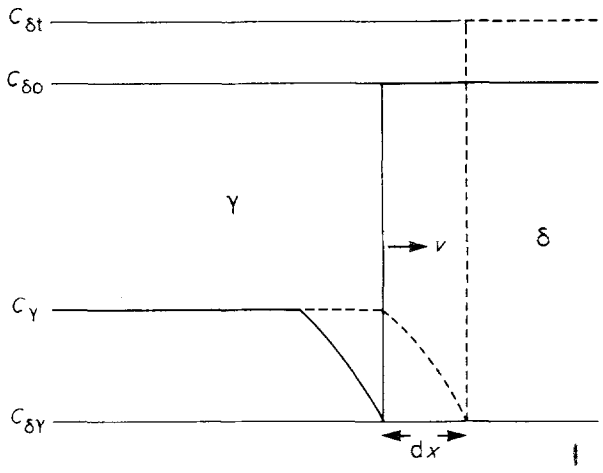

Figure 12 Schematic model showing solute concentration profile across the δ/γ interface during the dissolution of the δ-ferrite.

partially expected as the diffusivity at the δ/γ or in the δ-ferrite is approximately 100 times faster than that in austenite. The discrepancy between the experimental and the theoretical δ/γ migration distance is probably due to the fact that the reaction is unlikely to be controlled by the diffusion of a single element but will be controlled by the diffusion/interaction between a number of solute components.

4.3. Effect of compositional factors on the δ-ferrite stability

The mean composition of the δ-ferrite in the as-welded and different aged conditions have been plotted on the 700 °C isobaric section of the Fe–Cr–Ni–Mo quarternary [15], Fig. 13a–c.

In the as-welded condition, all the deposits lie in the δ + σ + γ and γ + σ of the 700 °C isobaric section of the phase diagram, Fig. 13a. Ageing for 0.5 h at 700 °C, in all cases resulted in significant shifts in the local composition of the δ-ferrite in relation to the phase boundaries, Fig. 13b. From these compositional studies combined with the metallographic and X-ray diffraction data, a number of trends in behaviour are apparent.

(i) In the 17Cr–8Ni–2Mo deposits, when the carbon content is above 0.07 wt % and the δ-ferrite levels are below 6%, the precipitation of $M_{23}C_6$ carbides deplete the δ-ferrite of Cr + Mo which results in a shift in composition of the δ-ferrite towards the γ + σ/γ phase boundary. This tends to encourage the formation of austenite in preference to the σ phase intermetallic. For example in BW13 and BW24, transformation of the δ-ferrite was predominantly to austenite with only small amounts of intermetallic formed after ageing in excess of 1000 and 3000 h, respectively. In BW17, the carbon level (0.077 wt %) is effectively diluted by the high volume fraction of δ-ferrite (11.4%) or high δ/γ boundary area. Consequently, there is insufficient carbon available to stabilize the δ-ferrite. This results in high residual levels of Cr + Mo (with the local composition of the δ-ferrite lying close to the δ + σ + γ/γ + σ phase boundary) and consequently rapid transformation to intermetallic.

(ii) In the 19Cr–12Ni–2Mo deposit (BW20), the low carbon levels combined with the high residual levels of Cr + Mo encouraged the rapid formation of intermetallic σ phase, the local composition of the δ-ferrite was lying in the δ + σ + γ region.

The strong influence of carbon on the δ-ferrite composition and its subsequent transformation, by the scavenging action of carbon for Cr + Mo and the effect of δ-ferrite level are illustrated in Fig. 14. This shows that the carbon content necessary to stabilize the δ-ferrite is proportional to the original δ-ferrite content and the reduction of Cr_{eq} after ageing. This is in agreement with other workers [5, 8, 16, 17] who have noted a similar stabilizing influence of carbon on the transformation behaviour. This can be modelled using the equation

$$C = \delta(\Delta Cr_{eq})m + A \qquad (4)$$

where C is the carbon content (wt %), δ is the original δ-ferrite level, ΔCr_{eq} is the % change in chromium equivalent and m and A are constants. From the ageing studies at 700 °C, m and A for the 17Cr–8Ni–2Mo are estimated to be -6.7×10^{-4} and 0.064, respectively.

The present studies suggest that in order to stabilize the 17Cr–8Ni–2Mo deposit, the carbon level should exceed 0.0165 wt % per unit volume of δ-ferrite.

4.3.1. δ-ferrite enrichment

After ageing for 70 h at 700 °C, STEM analysis showed that the δ-ferrite was steadily becoming enriched in Cr + Mo, Table II. Although the compositional scatter bands are large, the direction of change in the Cr and Mo levels have been plotted on the 700 °C isobaric section of the Fe–Cr–Ni–Mo quarternary, Fig. 13c. The increase in the compositional scatter band of the δ-ferrite at longer ageing times appears to be due to the variable extent of δ/γ interfacial migration in the δ-ferrite dendrites. The cause of this variability may be due to: (i) pinning of the δ/γ boundary by the $M_{23}C_6$ carbides; (ii) influence of alloy additions on grain-boundary mobility; (iii) differences in the δ/γ boundary structure.

The present studies show that the dissolution of the δ-ferrite results in an enrichment of the remaining δ-ferrite. These results are consistent with studies by Raghunathan *et al.* [18] who have reported additional enhancement in the Cr and Mo levels in the δ-ferrite on ageing at high temperature. The dissolution of the δ-ferrite and its transformation of the σ phase appears to be inter-related. The present studies suggest that during the δ-ferrite dissolution, the formation of intermetallics is controlled by the residual δ-ferrite enrichment process. A compositional controlled δ → σ transformation is further supported by the observation that, depending on the composition of the δ-ferrite, the transformation to intermetallic at 700 °C occurs in less than 1 h in BW20 (19Cr–12Ni–2Mo type) compared to 1000 h in BW13 (17Cr–8Ni–2Mo

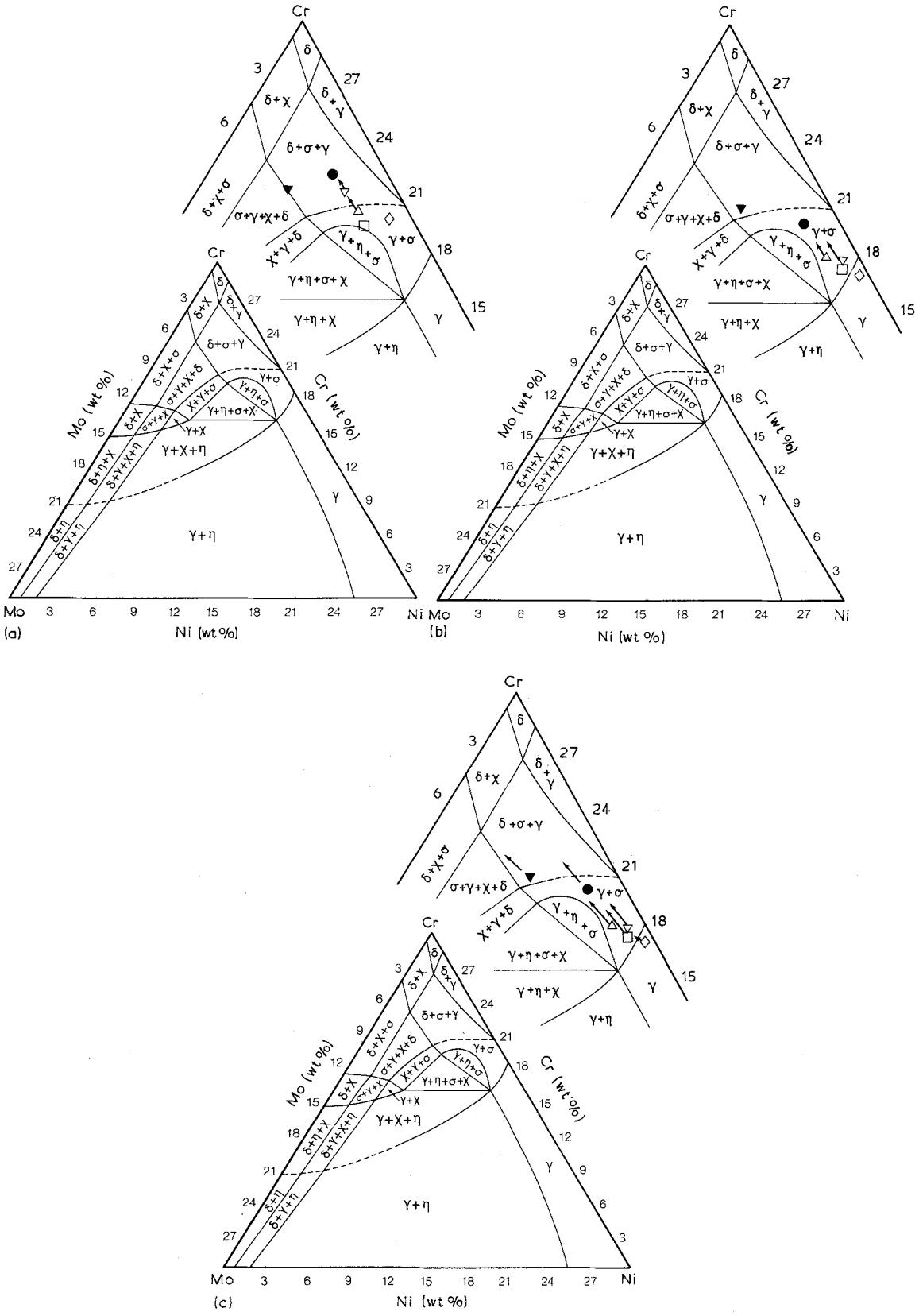

Figure 13 Composition of the δ-ferrite in relation to the Fe–Cr–Ni–Mo isobaric section at 700 °C: (a) as-deposited, (b) 0.5 h at 700 °C, (c) 70 h at 700 °C. (□) BW13, (▽) BW14, (●) BW17, (△) BW18, (▼) BW20, (◇) BW24; boundary curves (——) known, (– – –) inferred.

type). In addition, the weld metal with the highest local δ-ferrite Cr_{eq}, transformed fastest to intermetallics. The present work is consistent with other studies which have shown that the 19Cr–12Ni–3Mo weld metals have a greater tendency to transform to intermetallic phase than the leaner 17Cr–8Ni–2Mo types [19].

Vitek and David [9] have disputed the importance of compositional factors in controlling the $\delta \rightarrow \sigma$ reaction. However, it is perhaps significant that in their studies, in cases where the δ-ferrite had transformed to intermetallic, there was evidence of significant migration of δ/γ interface. The present studies show that the $\delta \rightarrow \gamma$ transformation is accompanied by significant

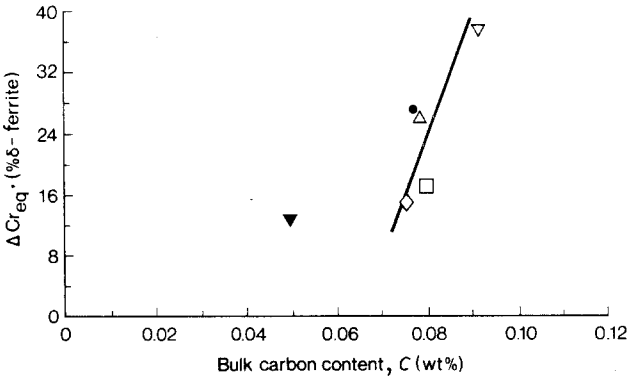

Figure 14 Change in Cr_{eq} of the δ-ferrite after ageing for 0.5 h at 700 °C relative to the bulk carbon content. (□) BW13, (▽) BW14, (●) BW17, (△) BW18, (▼) BW20, (◇) BW24; (□, ▽, ●, △) 17Cr–8Ni–2Mo, (▼) 19Cr–12Ni–2Mo, (◇) 17Cr–8Ni–1Mo.

diffusion of Cr and Mo across the δ/γ interface into the δ-ferrite. This has been shown to encourage the formation of intermetallics. It is significant that Vitek and David [20] in previous studies, have also noted this enrichment process but failed to appreciate the importance of the compositional enrichment on the δ → σ transformation. This is further supported by the STEM compositional profile across the σ/γ boundary, Fig. 10, which shows significant depletion of Mo and Cr adjacent to the interface.

Vitek and David [9] also noted that it was relatively rare to find a partially transformed δ-ferrite grain. This behaviour is consistent with the variable extent of δ/γ migration from δ-ferrite grain to grain. The failure of Vitek and David [9] to appreciate the role of compositional factors probably arises from their limited studies on only two weld metal compositions.

A number of different models such as PHACOMP [21] and the d orbital approach (M_d) [22] have been developed to predict the occurrence of sigma formation in Fe–Cr–Ni alloys. Senior [23] has attempted to apply the M_d approach to duplex 316 weld metals to predict differences in the susceptibility to intermetallic formation. However, this approach is too simplistic, as it is based on the bulk composition of the weld metal rather than the local micro-composition of the δ-ferrite. The M_d orbital approach will only indicate the relative tendency to form intermetallic at a fixed time.

The present studies have shown that the composition of the δ-ferrite is time dependent and that the propensity to form intermetallics increases with increasing time at temperature. It is believed that the formation of intermetallics is highly sensitive to the local micro-composition of the δ-ferrite. The PHACOMP and M_d approaches also take no account of the effect of carbon [17] which is known to influence strongly the local composition of the δ-ferrite and its tendency to transform to intermetallic.

4.4. Controlled residual additions

In the weld deposits BW13 and 14 containing the controlled residual element additions of Ti and Ti + B, ageing also resulted in the precipitation of a fine dispersion of MX particles in the austenite matrix, Fig. 10. Similar carbide dispersions have been observed by Vitek and David [20] in duplex 308 weld metal containing titanium additions of 0.5 wt %, but they are not well documented in weld metals containing trace levels of Nb + Ti + V. Ohmura *et al.* [24] have observed similar carbide distributions in weld metals containing trace level of vanadium. Based on thermodynamic data, these particles were thought to be M(C, N) carbonitrides, because the heat of solution of M(C, N) is less than that for either MC or MN [25]. The trace levels of Nb and V appear to have been derived from the titania added to the flux coatings. Titanium dioxide is obtained from rutile, a natural mineral containing approximately 93% TiO_2 but with smaller levels of niobium and vanadium oxides. However, because the niobium and vanadium oxides are more easily reduced in the welding arc than titanium dioxide, these small levels can become significant and the levels of Nb and V can exceed that of Ti, Table I.

It was not possible to determine the stoichiometry or the volume fraction of the MX phase formed on ageing, due to the lack of information on the composition of the precipitate. Studies by Andren *et al.* [26] of carbonitrides in austenitic steels containing additions of Ti, Nb and V have shown that the precipitates have a complex composition and frequently contain substantial amounts of chromium. In addition, it is known that the composition of the MX phase is sensitive to both time and temperature [26].

These MX precipitates may be important in controlling the creep properties of the weld metals [27].

5. Conclusions

1. During the δ → γ transformation, the δ-ferrite becomes progressively enriched in Cr, Mo and Si and depending on the local composition of the δ-ferrite, eventually transforms to austenite and/or intermetallic σ or χ. A transformation model has been developed in which solute diffusion via the δ/γ interface is shown to be the controlling mechanism.

2. The formation of intermetallics has been shown to be dependent on the residual levels of Cr, Mo and Si within the δ-ferrite and the enrichment process is controlled by the kinetics of δ-ferrite dissolution.

3. In agreement with other studies, the precipitation of $M_{23}C_6$ has been shown to denude the δ-ferrite of Cr and Mo, and lower the propensity for the formation of intermetallics. An empirical relationship has been derived which predicts the effect of carbon on the composition of the δ-ferrite. High levels of δ-ferrite have been shown to encourage the formation of intermetallics.

4. In the weld metals containing controlled residual additions of Ti and Ti + B, ageing resulted in the precipitation of a fine MX dispersion in the austenitic matrix.

Acknowledgements

This work was carried out in conjunction with Marchwood Engineering Laboratories (formerly of

the CEGB) and the authors are grateful to the laboratory manager for the provision of technical facilities. The X-ray diffraction analysis was performed by Mr J. Weaving. Acknowledgement is made of financial support by SERC CASE award SB101 for one of the authors (JJS).

References

1. B. WEISS and R. STICKLER, *Metall. Trans.* **3** (1972) 851.
2. F. R. BECKITT, *JISI* **207** (1969) 632s.
3. J. K. L. LAI, *Mater. Sci. Engng* **58** (1983) 195.
4. F. V. ELLIS and J. E. BYNUM, in "International Conference on Advances in Life Prediction Methods", edited by D. A. Woodford and J. R. Whitehead (ASME, New York, 1983) p. 337.
5. J. M. LEITNAKER, *Welding J. Res. Suppl.* **61** (1982) 9s.
6. R. A. FARRAR and R. G. THOMAS, *J. Mater. Sci.* **18** (1983) 3461.
7. J. WEGRZYN and A. KLIMPEL, *Welding J. Res. Suppl.* **60** (1981) 146s.
8. T. P. S. GILL, M. VIJAYALAKSHMI, J. B. GNANAMOORTHY and K. A. PADMANABHAN, *ibid.* **65** (1986) 122s.
9. J. M. VITEK and S. A. DAVID, *ibid.* **65** (1986) 106s.
10. S. A. DAVID, *ibid.* **60** (1981) 63s.
11. W. E. VOICE and R. G. FAULKNER, *J. Mater. Sci.* **22** (1987) 4221.
12. A. F. SMITH, *Metal Sci.* **9** (1975) 375.
13. *Idem., ibid.* **10** (1976) 418.
14. J. K. L. LAI, "Phase Transformations", Spring Residential Conference, Institution of Metallurgists, Series 3, **2** no. 11, (1979) Paper 1201-79-Y.
15. C. J. BECHTOLDT and H. C. VACHER, *J. Res. Nat. Bur. Stand.* **58** (1957) 7.
16. G. F. SLATTERY, M. E. LAMBERT and S. R. KEOWN, *Met. Tech.* **10** (1982) 373.
17. R. A. FARRAR, *J. Mater. Sci.* **22** (1987) 363.
18. V. S. RAGHUNATHAN, V. SEETHARAMAN, S. VENKADESAN and P. RODRIGUEZ, *Metall. Trans.* **10** (1979) 1683.
19. R. G. THOMAS and S. R. KEOWN, in "Conference on the Mechanical Behaviour and Nuclear Applications of Austenitic Stainless Steel at Elevated Temperatures", Varese, Italy (Metal Society, London, 1981).
20. J. M. VITEK and S. A. DAVID, *Welding J. Res. Suppl.* **63** (1984) 246s.
21. R. F. DECKER, in "Proceedings of the Steel Strengthening Symposium" (Zurich, Switzerland, 1969) p. 1.
22. M. MORINAGA, N. YAKAWA and H. EZAKI, *Phil. Mag. A* **51** (1985) 223.
23. B. A. SENIOR, *J. Mater. Sci.* **25** (1990) 45.
24. K. OHMURA, Y. OTOGURO, S. AOKI, S. SUZUKI, K. BANDO and T. ZAIZEN, in "Proceedings of the 2nd International Conference on Creep and Fracture of Engineering Materials and Structures" (Pineridge Press, Swansea, 1984).
25. F. B. PICKERING, in "Conference Proceedings Stainless Steel '84", Gothenburg, Sweden, Institute of Metals, Book 320 (Institute of Metals, 1984), p. 2.
26. H. O. ANDREN, A. HENJERED and L. KARLSSON, *ibid.*, Book 320, p. 91.
27. J. J. SMITH, PhD thesis, University of Southampton (1989).

Received 16 July
and accepted 1 August 1990